Received: 23 November 2022 | Revised: 21 February 2023 | Accepted: 14 March 2023

DOI: 10.1002/btpr.3341

BIOTECHNOLOGY PROGRESS

RESEARCH ARTICLE

Bioseparations and Downstream Processing

Continuous CTC separation through a DEP-based contraction–expansion inertial microfluidic channel

Md Sadiqul Islam | Xiaolin Chen

School of Engineering and Computer Science, Washington State University, 14204 NE Salmon Creek Ave, Vancouver, Washington, 98686, USA

Correspondence
Xiaolin Chen, School of Engineering and Computer Science, Washington State University, 14204 NE Salmon Creek Ave, Vancouver, WA 98686, USA.
Email: chenx@wsu.edu

Funding information
National Science Foundation, Grant/Award Number: 1917299

Abstract

The efficient isolation of viable and intact circulating tumor cells (CTCs) from blood is critical for the genetic analysis of cancer cells, prediction of cancer progression, development of drugs, and evaluation of therapeutic treatments. While conventional cell separation devices utilize the size difference between CTCs and other blood cells, they fail to separate CTCs from white blood cells (WBCs) due to significant size overlap. To overcome this issue, we present a novel approach that combines curved contraction–expansion (CE) channels with dielectrophoresis (DEP) and inertial microfluidics to isolate CTCs from WBCs regardless of size overlap. This label-free and continuous separation method utilizes dielectric properties and size variation of cells for the separation of CTCs from WBCs. The results demonstrate that the proposed hybrid microfluidic channel can effectively isolate A549 CTCs from WBCs regardless of their size with a throughput of 300 μL/min, achieving a high separation distance of 233.4 μm at an applied voltage of 50 V_{p-p}. The proposed method allows for the modification of cell migration characteristics by controlling the number of CE sections of the channel, applied voltage, applied frequency, and flow rate. With its unique features of a single-stage separation, simple design, and tunability, the proposed method provides a promising alternative to the existing label-free cell separation techniques and may have a wide range of applications in biomedicine.

KEYWORDS
circulating tumor cells, contraction–expansion channel, dielectrophoresis, inertial microfluidics, label-free separation

1 | INTRODUCTION

Cell separation from complex and heterogeneous biofluid is an essential prerequisite step for purifying target cells which can provide vital information for clinical diagnostics, cell-based therapies, drug development, and biomedical research applications.[1,2] Among different types of cells, CTC separation is regarded as an important intermediate step for early-stage cancer diagnosis and treatment. CTCs shed from primary tumor cells are spread through peripheral blood or lymphatic system to different organs of the human body which causes metastasis. While primary tumors hardly contribute to mortality, metastasis is the leading factor for the death of 90% of cancer patients.[3] A sampling of the primary tumor may not indicate the actual condition of metastasis. In contrast, the enumeration of CTCs in the blood can

effectively predict the stage of metastasis and help to monitor cancer treatment.[4,5] Therefore, isolation and detection of CTCs are vital for elucidating cancer growth as well as interpreting the metastasis characteristics. However, the number of CTCs found in a cancer patient's blood is extremely low which is 1–100 cells per mL or one count in 10^9 hematologic cells.[6,7] In addition to the rarity of CTCs in blood, heterogeneous morphology and significant size overlap with other blood cells turn the separation of CTCs into a challenging task.[7,8] To address this issue, efficient, rapid, and robust separation methods are required to achieve high-CTC detection accuracy with high purity and yield.

The separation of CTCs can be classified into two categories which are affinity-based/labeled approaches and label-free approaches. Biomarkers or labels are used in a labeled method to isolate CTCs from blood. Currently, there are various types of labeled methods such as FDA-approved cell search systems,[9] MagSweeper,[10] Magnetic activated cell sorting systems, and AdnaTest. However, in the labeled process, there is always a chance for contamination of CTCs, as these methods require different labels (e.g., membrane protein conjugated with particle-antibody) which are attached to the cells for enhanced separation.[11] In the case of the label-free method, different physical properties of CTCs such as the cell size, electrical properties, magnetic susceptibility, polarizability, shape, density, deformability, etc. are used for separation. As the label-free method only utilizes the cells' inherent properties, there is less chance of contamination of CTCs during the separation process.

Existing label-free macroscale cell separation methods such as centrifugation and flow cytometry are the most used techniques for cell separation. However, these methods suffer from low purity, high cost of installation, low throughput and require multiple passes for the full process.[12] Recently microfluidic technology has appeared with superior advantages compared to conventional macro-scale platforms in various fields such as heat transfer, multiphase flow, and nanofluids.[13–17] Microfluidic platforms are also used to separate cells from blood with high sensitivity of detection, reduced analysis time, simple geometry, less operating cost, and high throughput.[18] Microfluidic platforms can be broadly classified into two types: batch-wise cell separation and continuous cell separation. In the batch-wise method, a portion of the total sample volume of fluid is allowed to go through the separation process. After completing cell separation from that portion of the sample volume, the next portion of the sam-ple volume is processed and this procedure is repeated several times to achieve cell separation.[19] The batch-wise method may utilize field flow fractionation (FFF),[20] electrophoresis[21] or centrifugation[22] for cell separation. However, the batch-wise cell separation rate could be 20 times slower than the continuous cell separation.[23] In a continuous cell separation method, the sample volume of cells is injected continuously into the microfluidic cell separation device, thus it has less processing time.[19] Furthermore, continuous cell separation methods can be broadly divided into two categories: active methods and passive methods. In an active method, cell separation is achieved by using external force fields such as electric field, magnetic field, and acoustic field. Dielectrophoresis(DEP),[24] optical tweezer,[25] acoustophoresis[26] and magnetophoresis[27] are some well-known active methods.

Active methods can precisely manipulate cell trajectories in real time and they have high tunability. However, they have a significant drawback which is low throughput since the external force field must overcome the hydrodynamic force for effective separation.[28] Moreover, active devices are costly due to their requirement for an external force generator.

In contrast, passive methods do not require any external force field for their operation. Instead, passive methods achieve separation based on cell density, deformability, size, geometric parameters of the physical domain, and so on. Pinched flow fractionation (PFF),[29] deterministic lateral displacement (DLD),[30] hydrophoresis[31] and inertial microfluidics[32] are some of the well-recognized passive methods. Due to the capability of precise manipulation of cell trajectories, simple design, robustness, and high throughput, inertial microfluidics has recently gained much attention among all the passive methods.[33] In an inertial microfluidic channel, randomly dispersed cells take several equilibrium positions which are influenced by inertial forces acting on the cells.[32] However, the inertial microfluidics-based methods achieve separation based on the size of the cells, which limits their ability to isolate cells when the size of different cells overlaps among different cells. In addition, these techniques do not have as high tunability as active methods. To bridge this gap, the coupling of both active and passive methods to form a hybrid separation method has been reported in recent years.

Various hybrid microfluidic techniques have been studied by different research groups. The hybrid techniques have higher sensitivity, multiplexed separation capability, and enhanced tunability.[28] Aghaamoo et al.[34] combined DLD with DEP for the separation of CTCs from WBCs. However, the reported throughput in the device is significantly low, which is 2 μL/min. Moreover, the device has a chance of blood clogging due to the insulating posts in the physical domain. Shim et al. developed a cell separation method by coupling field flow-fractionation (FFF) with DEP where target cells are migrated downwards at the outlet due to the positive DEP force. On the other hand, the non-target cells are moved upward due to the influence of negative DEP force.[35] Yet, the proposed method uses the batchwise separation method which involves a complex design and adds difficulty to process the sample. Yan et al. developed a hybrid platform coupling hydrophoresis and DEP in which target cells are moved to the upper face of the channel and they achieve hydrophoretic ordering by interacting with upper channel grooves.[36] However, the developed method suffers from low throughput in the range of 2–4 μL/min and does not demonstrate the separation of similar-sized cells. Seo et al.[37] proposed a hybrid cell sorter combining hydrodynamics and magnetophoresis for improving separation efficiency where cells are separated using magnetic susceptibility. Yet, the proposed device separates different-sized cells only. Despite various combinations of the active and passive methods being developed, only a few works reported on combining inertial microfluidics with DEP. Zhang et al. developed a DEP-coupled serpentine inertial microfluidic channel for particle separation by modifying electric voltages.[38] However, the proposed

channel has a limitation in that it can only separate particles when there is a size difference among the particles. Moreover, the maximum lateral particle separation distance is only 29 μm for this channel. Alazzam et al. proposed a DEP-embedded inertial microfluidic channel that combined DEP that can separate green fluorescent protein-labeled MDA-MB-231 CTCs from a heterogeneous mixture of blood cells.[39] Yet, the proposed channel has a relatively low throughput of 6 μL/h. Recently, we reported a method combining inertial microflui-dics for the high-throughput separation of CTCs from the similar-sized WBCs using a zigzag channel.[40] However, the proposed method can separate cells with a low separation distance which can cause difficulties in controlling the precision of cell separation.[41]

Inertial microfluidics is employed using different types of channel geometry over the years, such as straight microchannel,[42] spiral microchannel,[43] and serpentine microchannel.[40] Although straight channels have the advantage of simple design and ease of operation, the channels cannot generate enough lift force for cell separation and require a large channel length.[33] Spiral channels have higher inertial lift force and can effectively separate different-sized particles due to the induced secondary flow.[44] However, the portion and deformability of large particles impact the recovery of small particles in spiral microchannels.[45] A serpentine channel can achieve well-defined focusing of particles with regulated inter-particle spacing due to its alternating curvature.[33] Yet, serpentine channels suffer from focusing small particles at high Reynolds numbers.[46] Due to the efficient particle focusing, separation, and mixing capability, the contraction–expansion (CE) channel has attracted the focus of researchers in the recent past as it allows inertial size separation by a force balance between the inertial lift and Dean drag forces in fluid regimes.[47] CE channel can separate both larger and smaller cells efficiently due to the microvortices which are formed inside the channel.[48,49] Moreover, high-throughput, increased separation distance, enrichment of cells and enhanced performance make the CE channels as an excellent choice for cell separation.[50–52] Lee et al.[53] reported a straight symmetric CE channel for the separation of breast cancer cells from WBCs with a recovery rate > 99% and a 97.4% blood cell rejection ratio. Bhagat et al.[54] developed an optimized straight CE channel by modifying channel aspect ratio, Reynolds number, and hematocrit with a CTC recovery rate of more than 80%. Although many studies are conducted on a straight CE channel, very few works on a curved CE channel have been reported in the past. Shamloo et al.[55] reported that a channel with one contraction section and two expansion sections can achieve particle separation in a shorter length than a straight contraction–expansion channel. However, the study did not demonstrate the effect of the number of CE on the separation of particles and the proposed device can only separate different-sized particles. Therefore, the study on curved CE channels with both the similar and different-sized particles or cell separation capability is still unreported.

Several studies are reported on the size range of CTCs and WBCs. Vona et al.[56] found from experiments that the mean tumor cell/WBC area ratio is 5.7 for Hep3B liver cancer cells, 4.5 for HepG2 liver cancer cells, 4.1 for LNCaP prostate cancer cells, and 2.8 for MCF-7 breast cancer cells. After comparing CTCs from breast cancer patients with WBCs, Hyun et al. concluded that the size of CTCs is generally larger or similar in size to WBCs.[57] Marrinucci et al.[58] reported an experiment with colorectal cancer patients and they found that the size of CTCs overlaps with the WBCs. According to these studies, it has been observed that the size of CTCs tends to be larger than white blood cells (WBCs) in the most cases. However, in several instances, the size of CTCs resembles that of WBCs.

To separate CTCs from both the similar and different-sized WBCs, a label-free method is proposed in this work coupling inertial microfluidics and DEP using a curved CE channel. To our best knowledge, no previous studies have reported combining inertial microfluidics with DEP in a curved CE channel for size-independent CTC separation. In this study, at first, the effects of the number of curved CE sections on cell separation are investigated. Then, the effects of applied voltage and flow rates on the separation distance are examined thoroughly. Cell migration characteristics in the lateral direction are also analyzed in detail to discover the underlying mechanism of cell separation in a DEP-coupled CE channel.

2 | RELATED THEORY

2.1 | Inertial migration

Inertial microfluidics is governed by the phenomena of lateral migration which determines an equilibrium position of randomly dispersed particles in a microchannel.[36] A laminar regime with a Reynolds number of 1–100 is typically observed in an inertial microfluidic channel. In an inertial microfluidic channel, several forces act on particles. Firstly, the particles travel along with the flow due to the influence of the viscous drag force (F_D). Secondly, the inertial migration of particles in a lateral direction of a microchannel depends on the net effects of two inertial forces which are the shear gradient lift force (F_{LS}) and wall-induced lift force (F_{LW}). The shear gradient lift force tends to migrate the particles to the wall from the channel center which depends on the parabolic velocity profile of the fluid. On the other hand, the wall-induced lift force (F_{LW}) arises from the disturbance of the flow field around particles and it causes the particles to migrate toward the center of the channel from the wall. These counteracting forces determine the equilibrium position of particles or cells in an inertial microfluidic channel. The resultant lift force on the particles can be expressed as follows[59,60]:

$$F_L = \frac{f_L(Re, z)\rho_f U_m^2 a_p^4}{D_h^2}, \quad (1)$$

$$Re = \frac{\rho_f U_m D_h}{\mu}, \quad (2)$$

where ρ_f, U_m, μ, a_p, D_h, and f_L are fluid density, the maximum velocity of the fluid, dynamic viscosity, cell diameter, the hydraulic diameter of the channel, and lift coefficient, respectively. The lift coefficient, f_L, depends on the channel Reynolds number (Re) and vertical position (z) within the channel cross section. It remains almost constant for Re < 100 and its approximate value is 0.5 in the most cases.[61]

Due to the presence of curvature downstream, a radially outward centrifugal force introduces a secondary flow that consists of two counter-rotating vortices which are known as the Dean vortices. The magnitude of the Dean vortices can be determined by a dimensionless number called the Dean number (De). The expression of Dean number is given as follows[62]:

$$De = \frac{\rho_f U_m D_h}{\mu}\sqrt{\frac{D_h}{2R}}, \quad (3)$$

where R is the radius of the curvature of the channel. The Dean flow introduces a force known as the Dean drag force (F_{Dean}) which is expressed as follows[63]:

$$F_{Dean} = 5.4\,10^{-4}\pi\mu a_p(De)^{1.63}, \quad (4)$$

where a_p is the radius of the particle. The combination of both the Dean drag force and inertial lift force determines the number of equilibrium positions of particles or cells. If the Dean drag force is stronger than the inertial lift force, then the cells will be focused as a single stream in the center of a microchannel. In contrast, the cells will take equilibrium positions near the two sidewalls of the microchannel.[61]

2.2 | Dielectrophoresis

Dielectrophoretic (DEP) force is induced due to the interaction between nonuniform electric fields and field-induced electrical polarization of particles. The particles which are immersed in an alternating electrical field will feel a time-averaged DEP force given by[64]:

$$F_{DEP} = 2\pi\varepsilon_{med}a_p^3 Re[K_{CM}(f)]\nabla E^2, \quad (5)$$

where ε_{med} and f are the permittivity of the suspension medium and the frequency of the applied nonuniform electric field of strength E, respectively. The term $Re[K_{CM}(f)]$ indicates the magnitude of the real part of the Clausius–Mossotti (CM) factor which can be expressed as follows:

$$K_{CM}(f) = \frac{\bar{\varepsilon}_{cell} - \bar{\varepsilon}_{med}}{\bar{\varepsilon}_{cell} + 2\bar{\varepsilon}_{med}}, \quad (6)$$

where $\bar{\varepsilon}_{cell}$ and $\bar{\varepsilon}_{med}$ are complex permittivity of cell and medium, respectively, and both of them are the function of the applied frequency. They can be further simplified as:

$$\bar{E}_{cell} = \varepsilon_{cell} - j\frac{\sigma_{cell}}{f}, \quad (7)$$

$$\bar{E}_{med} = \varepsilon_{med} - j\frac{\sigma_{med}}{f}, \quad (8)$$

where σ_{cell} and σ_{med} are the conductivity of the cell and medium, respectively. It can be observed from Equation (5) that the CM factor which depends on the applied frequency, determines the magnitude and direction of DEP force. A positive DEP force is generated when $Re(K_{CM}) > 0$, leading to the attraction of cells toward the area with a strong electric field. Conversely, if $Re(K_{CM}) < 0$, then DEP force becomes negative and cells will be pushed toward the lowest electric field gradient zone. However, if $Re(K_{CM}) = 0$, then it will create zero DEP force and cells will not change their initial position. Zero DEP force can be found at a particular applied frequency which is known as the cross-over frequency.

In a DEP-embedded inertial microfluidic device, cells are affected by both DEP and hydrodynamic forces. At first, the cells take equilibrium positions due to the influence of the inertial lift and Dean drag forces, and later the equilibrium positions are modified by the influence of the DEP force.

3 | NUMERICAL MODELING

For setting up the numerical model of the current DEP-based inertial technique, COMSOL 5.5 is used to characterize the flow behavior and cell separation. The fluid flow and electric field domain is solved using the AC/DC module of COMSOL Multiphysics. The following Navier–Stokes equation along with continuity equations[65] are used for solving the velocity field.

$$\rho\left(\frac{\partial v}{\partial t} + v\cdot\nabla v\right) = \nabla\cdot\left[-pI + \mu\left(\nabla v + (\nabla v)^T\right)\right] + F_v, \quad (9)$$

$$\nabla\cdot v = 0, \quad (10)$$

where ρ, v, μ and p are the fluid density, velocity, viscosity, and pressure, respectively. Here, F_v denotes the volume force which is created by the fluid–cell interaction.

To obtain the electric field E, the equations given below are solved:

$$E = -\nabla\varphi, \quad (11)$$

$$\nabla\cdot(\varepsilon_m E) = \rho_E, \quad (12)$$

$$\frac{\partial\rho_E}{\partial t} + \nabla\cdot(\sigma E) = 0, \quad (13)$$

where φ, ε_m, ρ_E, and σ are the electric potential, medium permittivity, net volumetric free charge density, and medium conductivity, respectively.

In the channel, cells are influenced by the combined effect of lift, drag, sedimentation, DEP, and Basset forces. These forces will determine the cell trajectory within the microchannel. Moreover, Newton's second law is applied by the transient solver to solve the motion of the cells in an incompressible liquid. The equation solved by the transient solver incorporating these forces is given below:

$$m_{cell}\frac{d}{dt}(v_{cell}) = F_{Drag} + F_{Lift} + F_{DEP} + F_{Sedim} + F_{Basset}. \quad (14)$$

Here, the Schiller–Naumann drag model is used for calculating the drag force which is defined below:

$$F_{Drag} = \frac{1}{\tau_p} m_{cell}(u - v_{cell}), \quad (15)$$

where u is the velocity of flowing fluid. The term τ_p is known as velocity response time which can be defined by the following equation:

$$\tau_p = \frac{4\rho_p d^2}{3\mu C_d Re}, \quad (16)$$

where ρ_p, C_d, and d are cell density, drag coefficient, and cell diameter, respectively.

When any particle or body moves through a fluid, a lagging boundary layer is developed with the change of relative velocity (acceleration). The Basset force arises due to this lagging boundary layer development, and it also accounts for the viscous effects of the fluid. The ratio of the Basset force to the Stokes drag with constant acceleration can be derived[66] from $R_{bs} = \sqrt{\frac{18\rho_m \tau_s}{\pi \rho_p t}}$. Here, τ_s is known as Stokes relaxation time. In our study, the medium density, $\rho_m = 1000\ kg/m^3$ and cell density, $\rho_p = 1050\ kg/m^3$ are considered.[67] As the ratio of medium density to cell density is very small, Basset force is negligible compared to the drag force. Moreover, the sedimentation force can be considered as $F_{Sedim} = \frac{4}{3}\pi r^3 g(\rho_p - \rho_m)$, where r is the radius of the cell and g is the acceleration due to the gravity.[67] As the value of cell density and medium density is close to each other, we can also ignore the sedimentation force in the current study.

The volume force discussed earlier is created due to the fluid cell interaction which is equal to the magnitude of the total drag force and acts in the opposite direction to the drag force. The volume force is defined as follows:

$$F_V(r) = \sum_{i=1}^{n} F_{Drag,i}\delta(r - q_i), \quad (17)$$

where r, δ, q_i, and n are the position of the cell, Dirac delta function, position vector, and the total number of cells, respectively.

DEP force generated by the nonuniform electric field can be found using Equation (5). However, the cells are composed of different elements such as cytoplasm, cell nucleus, and cell membrane which determine the dielectric behavior of cells. To find out the characteristics of biological cells, an equation of equivalent complex permittivity of cells is utilized which is derived from a single shell model.[68] According to the model, the equation of equivalent complex permittivity of cells is defined as:

$$\bar{\varepsilon}_{cell} = \bar{\varepsilon}_m \frac{\left(\frac{r}{r-d}\right)^3 + 2\frac{\bar{\varepsilon}_i - \bar{\varepsilon}_m}{\bar{\varepsilon}_i + 2\bar{\varepsilon}_m}}{\left(\frac{r}{r-d}\right)^3 - \frac{\bar{\varepsilon}_i - \bar{\varepsilon}_m}{\bar{\varepsilon}_i + 2\bar{\varepsilon}_m}}, \quad (18)$$

where r, d, $\bar{\varepsilon}_m$, $\bar{\varepsilon}_i$, and $\bar{\varepsilon}_{cell}$ are the cell radius, membrane thickness, complex permittivity of the membrane, the complex permittivity of cytoplasm, and equivalent complex permittivity of the cell, respectively.

To solve the numerical model, GMRES iterative solvers are used. The viscosity and density of the buffer solution are considered the same as water. A fully developed fluid velocity profile is used for the inlet with the no-slip condition at the walls. For the outlet, a zero static pressure is applied and the time step of 1×10^{-5} s is chosen for each simulation.

4 | VALIDATION

For the validation of the study, CE geometry is developed with the parameters reported by Lee et al.[69] Figure 1 is showing the validation results in which the probability density of particle position from the simulation is compared with the experimental results using 4 μm particles. The correlation coefficient and root mean square error (RMSE) between the experiment and simulation are 0.87 and 0.07, respectively which means the simulation result significantly aligns with the experimen-tal data.

The cell trajectory in the fluid domain is determined by discretizing the domain using tetrahedral meshes. Moreover, a mesh independence test is performed to improve the accuracy of the mesh and a grid number of 500142 is used for this study.

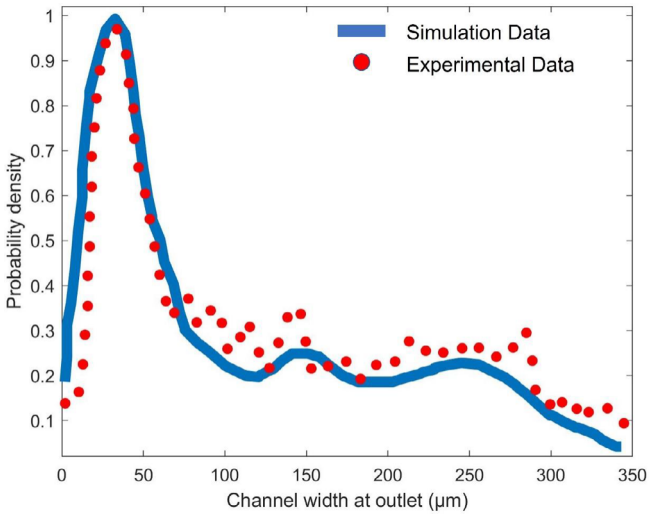

FIGURE 1 Comparison between the simulation and experimental data reported by Lee et al.[68] for 4 μm particles. Here, red color indicates the experimental data and blue color indicates simulation data. The probability density of particle position obtained from simulations is evaluated and compared with experimental results for 4 μm particles. The correlation coefficient and root mean square error (RMSE) are utilized to quantify the agreement between the experimental and simulated data, yielding a correlation coefficient of 0.87 and an RMSE of 0.07.

5 | OPERATING PRINCIPLE

In this study, a curved array of contraction and expansion microchannel is used to separate the CTCs from WBCs from blood. A sharp change of cross-sectional area is utilized in the channel which makes the fluid stream follow a curved path. When fluid enters the contraction region from the expansion section upstream, the flow accelerates. Due to the centrifugal effect, a secondary flow is induced in the contraction region which is known as the Dean flow. In contrast, the fluid decelerates while flowing through the expansion region from the contraction section due to the large cross-sectional area. Therefore, the effect of the Dean flow is offset by the deceleration. A shear-induced lift force is formed throughout the channel which tends to push the cells toward the center of the channel from the sidewall. In addition to shear-induced life force, a wall-induced lift force also prevails throughout the channel which tries to force the cells toward the center of the channel from the sidewall. However, in the contraction region, the shear-induced lift force is stronger than in the expansion region.[53] Therefore, the cells take an equilibrium position more quickly while passing through the contraction region. Both the Dean and inertial force are acted in the contraction region. Therefore, in our channel, planar interdigitated electrode arrays are placed outside of the inner sidewall of the contraction region to generate DEP force for cell separation.

In our proposed method, a sheath flow is used to pinch both CTCs and WBCs toward the inner sidewall of the channel. An AC electric field having a crossover frequency of CTCs is applied = when the focused cells are reached near the inner side of the contraction region. Due to the applied crossover frequency, the CTCs will not be affected by the generated DEP force. The relative displacement of CTCs and WBCs will be determined by the strength of lift force, F_L, and F_{DEP} which are shown in Equations (1) and (5), respectively. Experiencing negligibly small DEP force, CTCs will remain near the inner sidewall. However, the WBCs will feel strong DEP force and they will move toward the outer sidewall of the channel.

The CE microchannel consists of seven curved rectangular expansion sections and six curved rectangular contraction sections. As shown in Figure 2, each curved rectangular expansion section has a width of 350 µm and a height of 50 µm. On the other hand, each curved rectangular contraction section has a width of 50 µm and a height of 50 µm. The outer radius of this channel is 2500 µm from the center of the channel. The interdigitated electrodes are attached to the outside of the inner sidewall of the contraction region and there is a gap between each electrode. There are two inlets in the channel, one of them is used for sheath flow and another one is for the sample flow. In our study, A549 cells are considered representative of CTCs. Granulocytes are used as the representative of WBCs due to their significant size overlap with A549 CTCs and they are also the most abundant WBCs in a human body.[70,71] Both the similar-sized WBCs and different-sized WBCs have been used in our study. As the size of CTCs size is usually larger than WBCs,[56–58] smaller-sized WBCs are considered representative of different-sized WBCs. Although there is a significant size overlap, both CTCs and WBCs have different

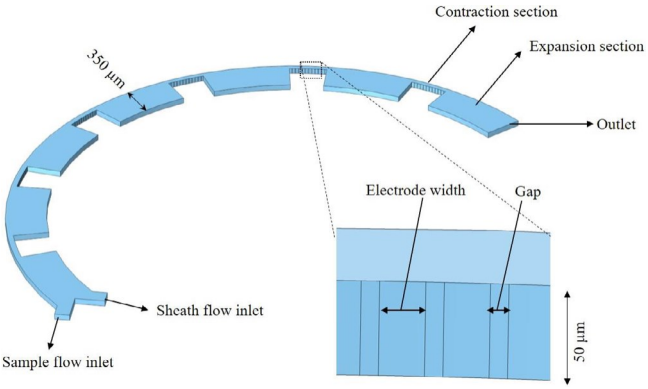

FIGURE 2 CE channel geometry for the proposed CTC separation method. The microfluidic channel design includes curved rectangular expansion and contraction sections, each with a height of 50 µm. The width of the expansion sections is 350 µm, while the width of the contraction sections is 50 µm. The outer radius of the channel is 2500 µm from the center of the channel. Interdigitated electrodes are located on the outside of the inner sidewall of the contraction section, with a gap between each electrode. The channel has two inlets, one for the sheath flow and the other for the sample flow.

dielectric properties, and can thus be separated by using DEP with appropriate cross-over frequency.

The size range of cells along with their dielectric properties are mentioned in Table 1. As mentioned in the theory section, the Clausius–Mossotti (CM) factor which depends on the applied frequency determines whether negative DEP(nDEP), positive DEP(pDEP), or zero DEP force will work on a particular type of cells. In the current study, we set it up in such a way that a negative DEP force will work on WBCs and CTCs will have a zero DEP force as the applied frequency is set to the crossover frequency of CTCs. Figure 3 shows the variation of the CM factor against the applied frequency where the mean cross-over frequency of the CTCs is shown by the black vertical line which is 65 kHz.

6 | RESULTS AND DISCUSSION

6.1 | Effects of the number of CE sections

Geometry plays a vital role in particle separation migration characteristics. In the case of CE microchannel, the number of CE sections has an important role in cell separation, and the selection of an optimum number of CE sections is a critical factor for increasing separation efficiency. To study the effect of the number of CE sections, a sheath flow of 110 µL/min and a sample flow of 10 µL/min is considered. Moreover, CTCs and only different-sized WBCs are used for mixing in the sample flow. Additionally, no DEP force is used for the selection of an optimum number of CE sections.

Initially, the separation of cells in the channel is not observed when only one CE section is used. However, the addition of one CE

TABLE 1 Dielectric and physical properties of CTCs and WBCs.

Cell type	Radius r (μm)	Crossover frequency f_c (kHz)	Cytoplasm conductivity σ_{cp} (S/m)	Cytoplasm complex permittivity $\bar{\varepsilon}_{cp}$	Membrane thickness d(nm)	Membrane conductivity σ_m (S/m)	Membrane complex permittivity $\bar{\varepsilon}_m$
A549 CTCs	7.75 ± 0.25	65 ± 2.5	0.99	100	10	2 10^6 1	27
Similar-sized WBCs (granulocytes)	7.75 ± 0.1	156.65 ± 2	0.72	111	5	10^6	5.54
Different-sized WBCs (granulocytes)	3.75 ± 0.25	325 ± 21	0.72	111	5	1 10^6	5.54

Note: Dielectric properties of the cell beads with a medium conductivity of 0.055 S/m and relative permittivity of 80 for both CTCs and WBCs.

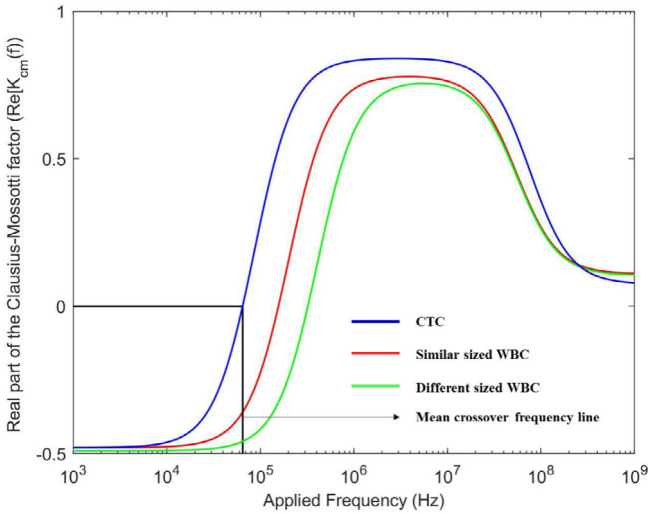

FIGURE 3 The variation of the CM factor for different cells with the applied frequency, where the black vertical line represents the mean crossover frequency of the CTCs at 65 kHz. The DEP force can be negative (nDEP), positive (pDEP), or zero, depending on the value of the CM factor. We designed the experiment to apply a negative DEP force on WBCs and a zero DEP force on circulating tumor cells (CTCs) by setting the applied frequency to the crossover frequency of CTCs.

section at a time results in an increasing number of CE sections, leading to the separation of cells, as demonstrated in Figure 4. Cell separation is initially observed when using four CE sections, and the distance of cell separation increases gradually up to seven CE sections. With further increase in the number of CE sections, the distance between separated cells decreases.

This study investigates the separation characteristics of several CE sections, up to a maximum of 13 sections. A CE channel induces a secondary transverse flow, known as the Dean flow, in the contraction section, where two counter-rotating vortices are formed in the upper and lower regions. Both the sample and sheath flow experience the Dean flow while passing through this section. In addition to the Dean flow, inertial lift forces influence the cells throughout the channel. Therefore, the equilibrium positions of the cells at the outlet are determined by the balance between the inertial lift and the Dean force.

The inertial lift force described by Equation (1) is directly proportional to cell diameter, making CTCs more strongly influenced by this force due to their larger size. This force causes the cells to move toward the inner side of the channel, as shown in Figure 5. Conversely, the Dean force dominates in different-sized WBCs due to their smaller size and acts to push the cells to the outer wall. The WBCs are observed to gradually migrate toward the outer wall with an increase in CE sections from 4 to 7. However, after Section 7, the WBCs move gradually toward the inner side of the outlet and cannot be separated from CTCs, following the rotational fluid movement of the Dean vortices for 8 to 13 CE sections. From the results shown in Figure 5, it is evident that seven CE sections provide the maximum separation distance between CTCs and WBCs with complete focusing. As a result, 7 CE sections are selected for the CE channel geometry for this study. The overall separation length of the channel with seven CE sections is 0.8 cm and only few studies are reported that can achieve separation in such shorter distance. Yuan et al. reported an asymmetrical expansion–contraction cavity arrays for elasto-inertial particle focusing with a channel length of 5 cm.[72] Warkiani et al. developed a high-aspect ratio microchannels for malaria detec-tion having channel length of 2 cm.[73] Sim et al. demonstrated a size-based separation of microspheres using multiple series of CE microchannels having length of 2.4 cm.[74] Wu et al. successfully isolated microparticle and blood cell separation in a straight channel with local microstructures with a length of 11.2 cm.[75]

6.2 | Effects of the applied voltage on the lateral migration of cells

Following the selection of an appropriate number of CE sections, the effect of applied voltage on cell separation is extensively investigated. As the DEP is integrated into the proposed CE microchannel, the applied voltage plays a vital role in controlling particle trajectory. The magnitude of the DEP force is a function of electric field intensity, which depends on the applied voltage's magnitude, as evident from Equation (5). In this study, interdigitated electrodes with a width of 10 μm and a spacing of 5 μm are attached to the outer surface of the inner contraction section of the channel, which generates a nonuniform electric field for DEP force. Due to the sheath flow, all cells move toward the inner side of the contraction region where they experience the DEP force. The applied electric field only affects WBCs, as CTCs are not influenced by the frequency set to the

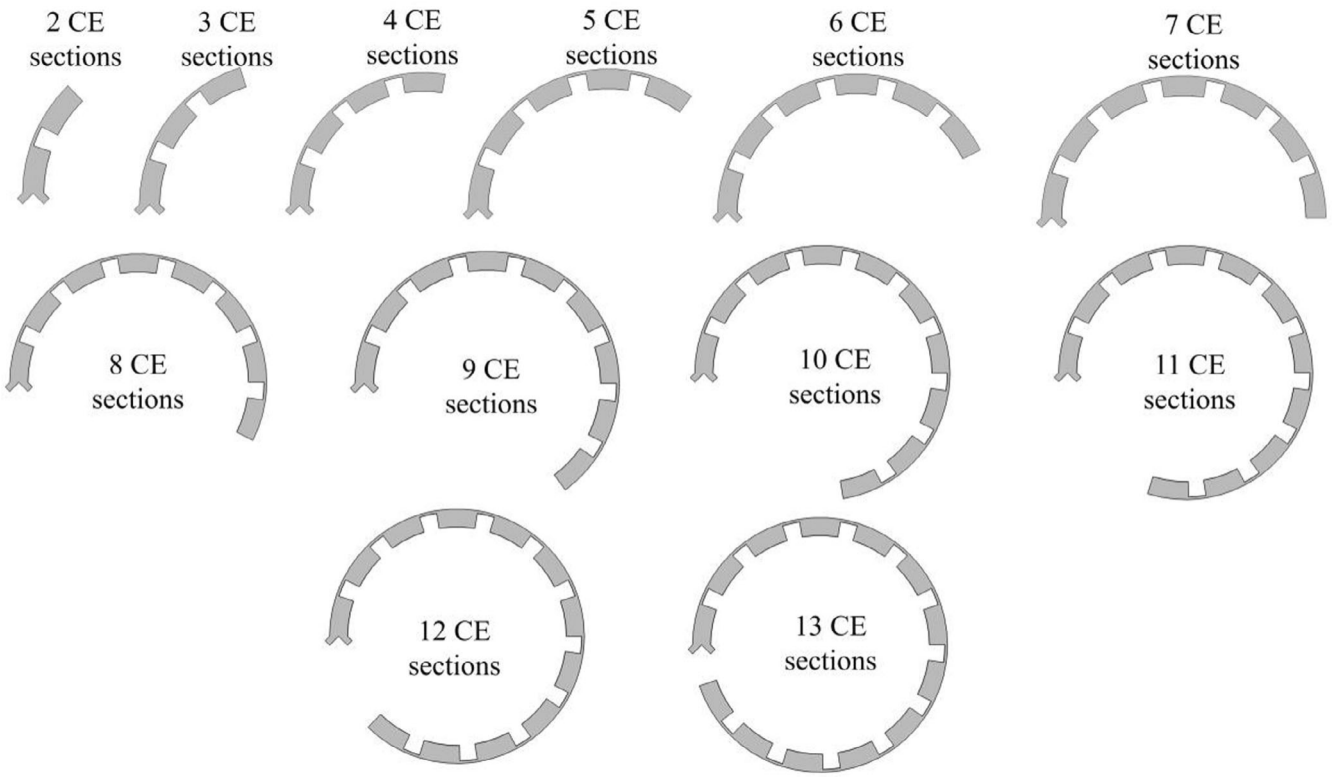

FIGURE 4 Cell separation for various CE sections. The number of CE sections increased gradually from 2 to 13 to find the best CE section with maximum cell separation distance. This study examined the impact of the number of CE (curved expansion) sections on the efficiency of particle mixing. To achieve this, a sample flow rate of 10 μL/min and a sheath flow rate of 110 μL/min were used. The sample flow consisted of CTCs and various sizes of WBCs. The experiment was conducted without applying any dielectrophoretic (DEP) force to assess the optimal number of CE sections for effective particle separation.

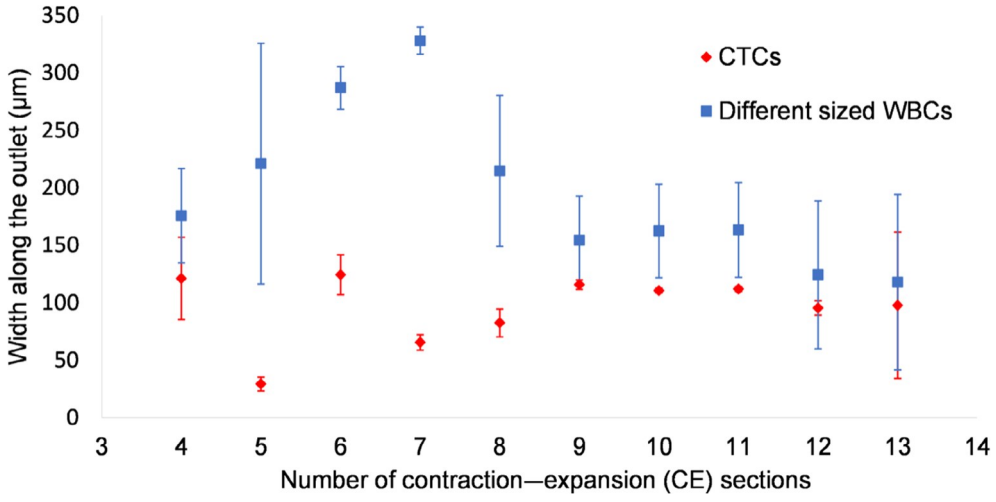

FIGURE 5 Variation of cell separation distance along the width of the outlet against the increase of the number of CE sections. The error bars indicate the width of the focusing positions of the cells. It is observed that with an increase in the number of curved expansion (CE) sections from 4 to 7, WBCs move gradually toward the outer wall. Beyond 7 CE sections, the WBCs start to migrate toward the inner side of the outlet, following the rotational fluid movement of the Dean vortices, and cannot be separated from CTCs. It is found that 7 CE sections provide the maximum separation distance between CTCs and WBCs, with complete focusing.

crossover frequency of CTCs. Therefore, only WBCs are affected by the applied electric field and pushed toward the outer side of the channel.

Figure 6 shows the lateral position of cells along the width of outlet with different peak-to-peak applied voltage with a flow rate of 120 μL/min. For each applied voltage we used 30 CTCs, 30 similar-

sized WBCs and 30 different sized WBCs (Total 90 cells). Each type of cells takes different focusing position along the width of the outlet. The error bars indicate the width of the focusing positions of the cells. The results indicate that, initially the CTCs and similar-sized WBCs tend to stay close to the inner sidewall of the outlet, while different-sized WBCs tend to take a position near the outer sidewall. However, as the applied voltage increases from 5 V_{p-p} to 15 V_{p-p}, similar-sized WBCs move outward and different-sized WBCs begin to focus near the center.

For the voltage of 15–25 V_{p-p}, both the different-sized WBCs and similar-sized WBCs overlap with each other. The similar-sized WBCs experience higher DEP force compared to different-sized WBCs due to their difference in diameter. If the voltage is further increased, the similar-sized WBCs move more toward the outer side. On the other hand, the spread of different-sized WBCs is reduced with the increase of applied voltage near the center of the outlet. At the voltage of 35 V_{p-p}, similar-sized WBCs are completely separated from different-sized WBCs. Moreover, both the similar-sized WBCs and different-sized WBCs shrink into a single focusing streak at the voltage of 35 V_{p-p}. Therefore, 35 V_{p-p} is the critical separation voltage for the flow rate of 120 µL/min. At the critical voltage, the average distance from CTCs to different-sized WBCs and the similar-sized WBCs are 89.7 µm and 155.3 µm, respectively. It is also noted that at the voltage of 50 V, the maximum separation distance can be obtained. Figure 7 shows the trajectories of CTCs and WBCs at the applied voltage of 50 V_{p-p}. At the maximum separation voltage, the average distance from CTCs different-sized WBCs and similar-sized WBCs is 94.5 µm and 233.4 µm, respectively. Further increase of applied voltage has a negligible effect on separation distance which can be seen in Figure 6 for the applied voltage of 55 V_{p-p}. The separation distance achieved in our channel is higher than the most of the existing cell devices which ensures higher separation precision.[46] Rafeie et al. successfully separated blood plasma with separation distance less than 70 µm in a slanted spiral microchannels.[76] Cruz et al. demonstrated separation of bacteria in a curved microchannel having separation distance less than 20 µm with other cells.[77] Recently, Khan et al. developed a serpentine microfluidic channel to separate breast cancer cells from WBCs with a separation distance less than 40 µm.[40] Although cells are completely separated at the critical voltage, any applied voltage between the critical and maximum separation voltage can be selected according to the desired cell separation distance. It is also observed that the CTCs remain at the inner sidewall of the outlet for any applied voltage, as the CTCs are not affected by DEP force due to the applied crossover frequency.

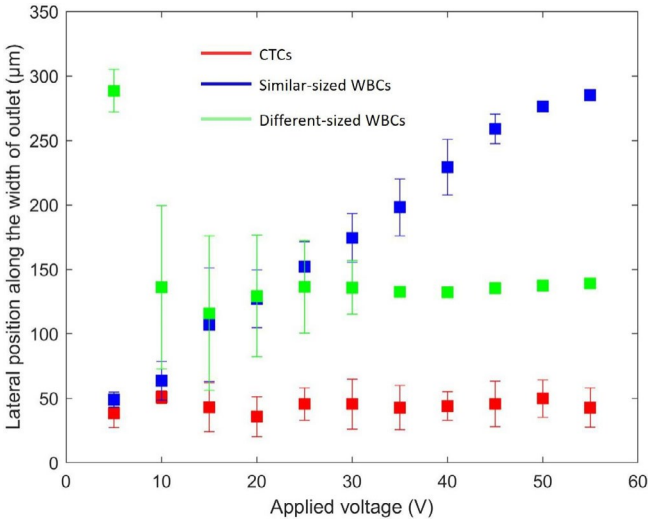

FIGURE 6 As the applied voltage is increased from 5 V_{p-p} to 15 V_{p-p}, it is observed that similar-sized WBCs move outward, while different-sized WBCs start to concentrate near the center. Between 15 and 25 V_{p-p}, it is found that both the different-sized and similar-sized WBCs overlap with each other. At 35 V_{p-p}, the similar-sized WBCs are entirely separated from the different-sized ones, which are shrank into a single focusing streak. This finding indicates that 35 V_{p-p} was the critical voltage for achieving optimal separation at the flow rate of 120 µL/min. It is worth noting that the maximum separation distance was obtained at a voltage of 50 V_{p-p}.

6.3 | Effects of flow rate on cell separation

Flow rate is crucial for determining the throughput of a cell separation device. In the current study, the flow rate is varied to investigate its

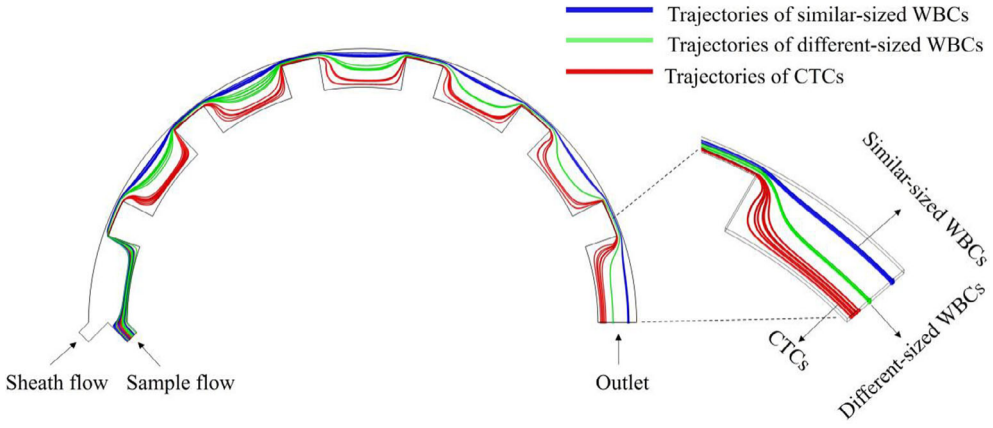

FIGURE 7 The cell trajectories along the CE channel for applied voltage of 50 V_{p-p} for the flow rate of 120 µL/min. The red, green and blue color represents the trajectories of CTCs, different-sized WBCs and the similar sized WBCs, respectively. Here, the average separation distances between CTCs and different-sized WBCs, and between CTCs and the similar-sized WBCs are 94.5 µm and 233.4 µm, respectively.

effect on the critical voltage of cell separation. It is found that the magnitude of the critical voltage increases with the increase of the flow rate. Figure 8 shows the critical voltage required for cell separation at various flow rates. For a flow rate of 120, 150, 180, 210, 240, 270, and 300 µL/min, the critical required are 35, 45, 52, 60, 68, 75, and 80 $V_{p\text{-}p}$ respectively. Moreover, a linear trend between the flow rate and critical voltage is observed which means the critical voltage is almost linearly proportional to the flow rate. Equations (1), (3), and (4), demonstrate that both the inertial lift and dean drag forces depend on the Reynolds number which is proportional to the flow rate. Thus, both the inertial lift and Dean drag forces become stronger with the increase of the flow rate. To maintain a balance with the strong inertial and Dean drag force, a high-DEP force is required. For attaining higher DEP force electric potential must be increased throughout the channel.

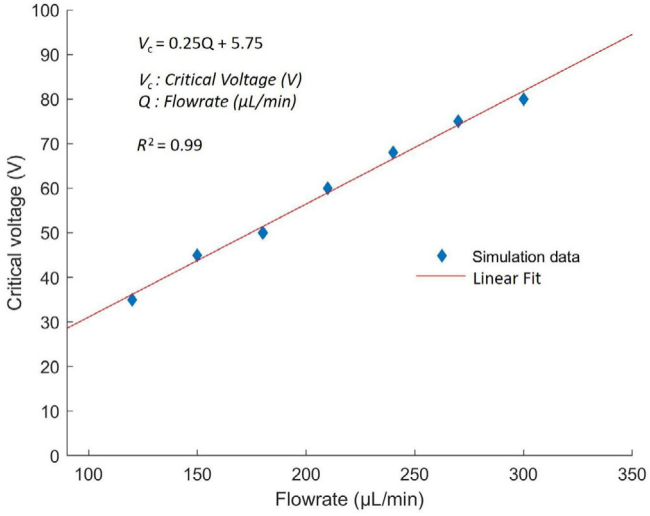

FIGURE 8 Variation of the critical voltage (peak-to-peak) against the flow rate. The simulation data is presented with a linear fit curve. Here R^2 is the coefficient of determination. The critical voltages necessary for separation at flow rates of 120, 150, 180, 210, 240, 270, and 300 µL/min are found to be 35, 45, 52, 60, 68, 75, and 80 V_{p-p}, respectively. A linear relationship is observed between the flow rate and critical voltage, indicating that the critical voltage is almost directly proportional to the flow rate.

However, at a high flow rate such as 330 µL/min, flow separation occurs at the edge of the contraction region. When the fluid enters the expansion region from the contraction region, a large vortex is induced due to the flow separation. As a result of the flow separation fluid velocity reduces significantly near the inner wall of expansion sections. Figure 9a shows the comparison of the effects of low flow rate and high flow rate in the channel.

At a low flow rate, the fluid velocity remains uniform throughout the expansion section. However, at a very high flow rate, the fluid velocity reduces significantly near the inner wall of the expansion section due to the vortex that is induced by the flow separation. The induced vortex which is shown in Figure 9b, creates additional lift force which pushes the CTCs toward the channel center from the inner wall. Moreover, this vortex reduces the radius of curvature of the streamline in the expansion region which decreases the separation distance between CTCs and WBCs. Therefore, a higher DEP force is required to push the WBCs toward the outer wall for increased separation distance. It is found that a flow rate greater than 300 µL/min would induce a very strong vortex in the expansion region and very high voltage is required to achieve cell separation. The achieved flow rate of 300 µL/min is greater than that of the majority of the previously reported DEP-based microfluidic channels. Aghaamoo et al.[34] reported a hybrid microfluidic device which can separate CTCs from

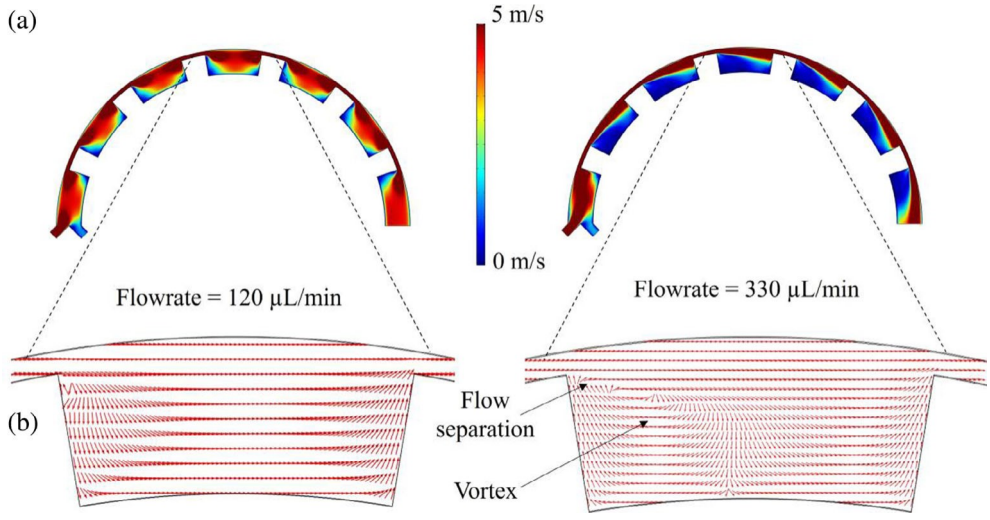

FIGURE 9 (a) Velocity contour plot for flow rate of 120 µL/min and 330 µL/min. At high flow rates, a vortex is generated due to flow separation, leading to a significant reduction in fluid velocity near the inner wall of the expansion section. (b) Effects of low and high flow rate on flow separation in the expansion sections. The vortex generated induces an extra lift force that moves the CTCs toward the center of the channel from the inner wall. Furthermore, this vortex causes a reduction in the radius of curvature of the streamline in the expansion region, resulting in a decrease in the separation distance between CTCs and WBCs.

WBCs at a flow rate of 2 μL/min. Yan et al.[36] achieved flow rate of 2–4 μL/min by combining hydrophoresis with DEP for cell separation. Alazzam et al.[39] proposed a DEP-embedded inertial microfluidic channel for the separation of MDA-MB-231 CTCs and the device attained a flow rate of 0.1 μL/min. Moon et al.[78] successfully demonstrated a microfluidic device coupling DEP with multi-orifice flow fractionation to with a flow rate of 126 μL/min.

From Figure 8, it is clearly observed that a higher applied voltage is necessary to achieve cell separation at a high flow rate while a low applied voltage is sufficient for the CTCs at a low flow rate. It is also observed that due to the short length of the proposed channel, the cells require a significantly short time for passing from the inlet to the outlet. For instance, for the flow rate of 120 μL/min, the cells take only 0.35 s to move from channel inlet to outlet and the moving time is less than 0.35 s for the high flow rates. Lu et al.[79] reported that short-term DEP exposure (1 min or less) with frequencies near the crossover frequency does not affect cell survival and proliferation. However, lengthy exposure (more the 5 min) to the crossover frequency may reduce cell survival. Due to the very short exposure time of cells to the electric field, it is expected that cell viability will not be affected during the separation process in our proposed channel.

6.4 | Cell migration characteristics

Cell migration characteristics depend on the combined effect of the inertial lift, Dean drag, and the DEP force. As the planar interdigitated electrodes are attached to the inner sidewall, the DEP force acts more strongly near the inner sidewall. The magnitude of the electric field gradually reduces from the inner sidewall to the outer sidewall which is shown in Figure 10a and the DEP force is generated from a non-uniform electric field at the contraction region that is shown in Figure 10b. The equilibrium position of CTCs is determined by the inertial lift and Dean drag force. CTCs are not affected by the DEP force, as the frequency of the applied electric field is set to the crossover frequency of CTCs. However, both the different and similar-sized WBCs will be affected by DEP force in addition to the inertial lift and Dean drag force.

Figure 11 a shows the migration characteristics of cells along the width of the contraction region of the channel. In this study, the minimum applied voltage for which CTCs, the similar-sized WBCs, and different-sized WBCs are separated from each other is defined as the critical separation voltage. Additionally, the voltage for which the cell separation distance becomes maximum is defined as the maximum separation voltage. In the case of CTCs, they remain near the inner channel wall due to the balance between the inertial and Dean drag force. However inertial lift force acts more strongly than the Dean drag force due to the large diameter of CTCs.

In the case of the different-sized WBCs, inertial lift force creates less effect on them due to their small diameter. Rather, the different-sized WBCs will be affected mostly by the Dean Drag force which tries to push them near the inner wall. However, the different-sized WBCs take position near the center due to the net interaction force between the Dean Drag force and inertial lift force. Figure 11b shows that initially at a low voltage, the equilibrium position of different-sized WBCs will be disturbed, and they have a tendency to move toward the center due to the Dean flow. Due to the balance between the DEP and the Dean drag force, they will take a position at the center with a wide spread. However, with the increase of applied voltage, the DEP force becomes stronger and the spread of different-sized WBCs starts to reduce gradually. At the critical voltage, different-sized WBCs are completely separated from the similar-sized WBCs and CTCs. For the similar-sized WBCs, they merge with the CTCs when there is no DEP force. When the DEP is applied, the similar-sized WBCs will be influenced more strongly than different-sized WBCs by the DEP force and the similar-sized WBCs will be pushed toward the outer wall. With the increase of the applied voltage, the similar-sized WBCs will be moving toward the outer wall and the width of the spread will be reduced at the same time. At the critical voltage, the CTCs will be completely separated from both the similar and different-sized WBCs. The equilibrium position of the similar-sized WBCs will be moved toward the outer wall slowly with the further

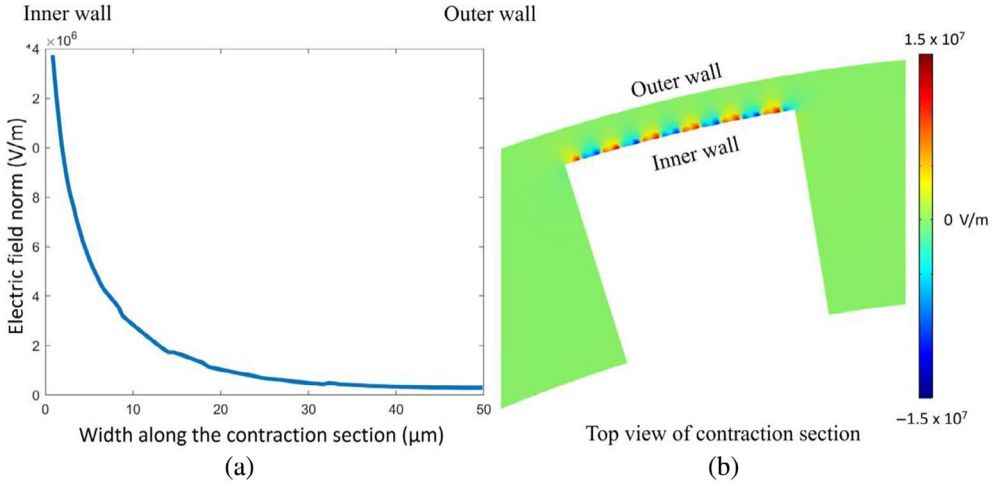

FIGURE 10 (a) Variation of electric field norm along the width of a contraction section. (b) The contour of electric field distribution in a contraction section for applied voltage of 50 V_{p-p}. Both figures indicate that the electric field strength diminishes progressively from the inner wall to the outer wall.

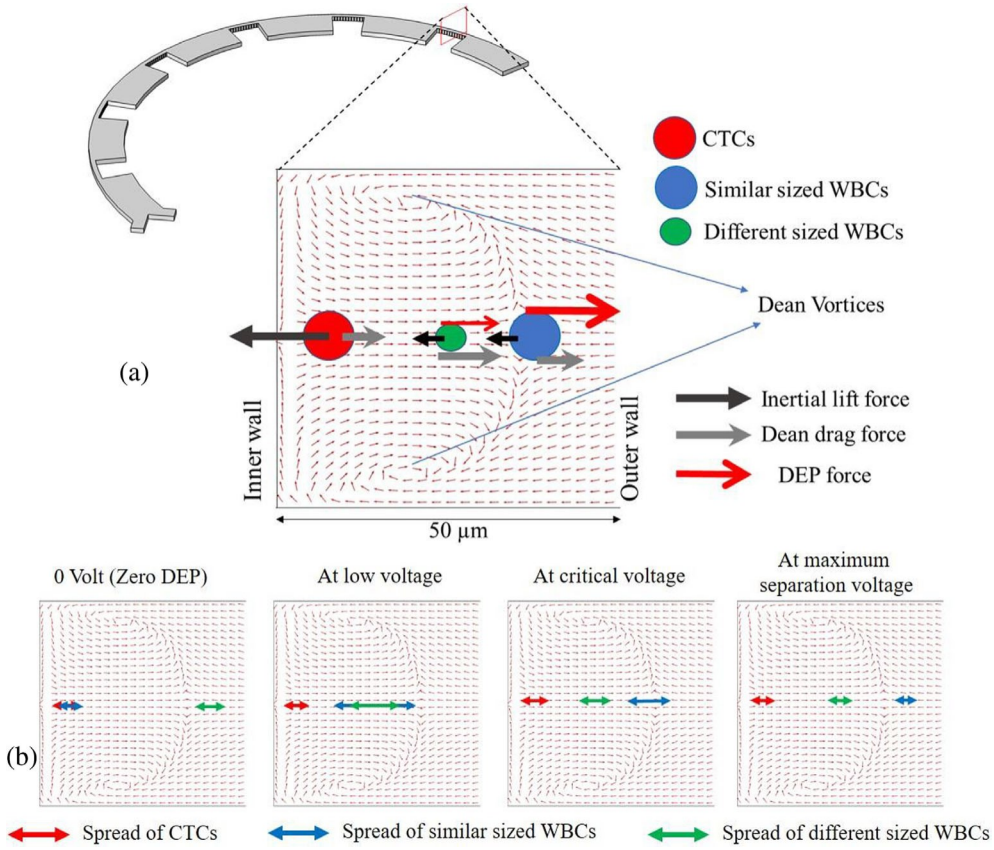

FIGURE 11 (a) Schematic of different forces acting on the contraction section. For CTCs, the equilibrium between the inertial and Dean drag force causes them to remain in proximity to the inner channel wall. Nevertheless, the inertial lift force predominates over the Dean drag force because of the substantial size of the CTCs. (b) Cell migration characteristics for different applied voltage. The red, blue, and green arrows indicate the focusing width of the cells. At a low voltage, the Dean flow induces a disturbance in the equilibrium position of WBCs with various sizes, making them move toward the channel center. However, the increase in the applied voltage amplifies the DEP force, leading to a gradual reduction in the spread of WBCs. At a critical voltage, WBCs with different sizes become entirely separated from WBCs with the similar sizes and CTCs. At the maximum separation voltage, both WBCs with different and the similar sizes align in a single focusing streak, and any additional increase in the applied voltage will not significantly alter the cells' position.

increase of the voltage. At maximum separation voltage, both the different and similar-sized WBCs will take a single focusing streak and further increase of applied voltage will not cause a significant change of position of cells.

7 | CONCLUSION

In this work, a hybrid CTC sorting method is proposed combining Dielectrophoresis with inertial microfluidics in a novel curved CE channel. CTCs are separated laterally from both different and overlapping-sized WBCs utilizing the leverage of the horizontal DEP, Dean drag, and inertial lift force. This method surmounts the shortcomings of the conventional size-based cell separation method as it exploits the advantage of both the size and dielectric properties of the cell for the separation of CTCs. The current study reveals that the CTC separation mechanism can be controlled effectively by modifying the number of curved CE sections, applied electric voltage, and flow rate. This hybrid microfluidic channel can achieve a throughput of 300 μL/min, while maintaining a high cell separation distance of CTCs and WBCs at the outlet.

7.1 | Future Perspectives

The proposed novel cell sorting platform can be expanded to enable the separation of specific target cells and particles from complex mixtures containing cell beads and other particles. This can be achieved through simple modifications to the applied electric field frequency, obviating the need for any alteration to the channel design. The unique feature of this platform to effectively sort distinct cell and particle types using a straightforward manipulation of the electric field frequency allows for potential broadened applications in the sorting of heterogeneous cell populations.

AUTHOR CONTRIBUTIONS

Md Sadiqul Islam: Conceptualization (equal); data curation (lead); formal analysis (lead); investigation (equal); methodology (equal); project

administration (supporting); resources (equal); software (equal); validation (equal); visualization (lead); writing – original draft (lead). Xiaolin Chen: Conceptualization (equal); funding acquisition (lead); investigation (equal); methodology (equal); project administration (lead); resources (equal); software (equal); supervision (lead); validation (equal); writing – review and editing (lead).

ACKNOWLEDGMENTS

This material is based upon work supported by the National Science Foundation under Grant No. 1917299.

CONFLICT OF INTEREST STATEMENT

The authors declare no conflict of interest.

DATA AVAILABILITY STATEMENT

Data available on request from the authors.

ORCID

Xiaolin Chen https://orcid.org/0000-0002-8760-6480

REFERENCES

1. Toner M, Irimia D. Blood-on-a-Chip. Annu Rev Biomed Eng. 2005;7(1):77-103. doi:10.1146/annurev.bioeng.7.011205.135108
2. Jackson EL, Lu H. Advances in microfluidic cell separation and manipulation. Curr Opin Chem Eng. 2013;2(4):398-404. doi:10.1016/j.coche.2013.10.001
3. Cristofanilli M, Budd GT, Ellis MJ, et al. Circulating tumor cells, disease progression, and survival in metastatic breast cancer. N Engl J Med. 2004;351(8):781-791. doi:10.1056/NEJMoa040766
4. Punnoose EA, Atwal SK, Spoerke JM, et al. Molecular biomarker analyses using circulating tumor cells. PLoS One. 2010;5(9):e12517. doi:10.1371/journal.pone.0012517
5. Nagrath S, Sequist LV, Maheswaran S, et al. Isolation of rare circulat-ing tumour cells in cancer patients by microchip technology. Nature. 2007;450(7173):1235-1239. doi:10.1038/nature06385
6. Mostert B, Sleijfer S, Foekens J, Gratama JW. Circulating tumor cells (CTCs): detection methods and their clinical relevance in breast cancer. Cancer Treat Rev. 2009;35(5):463-474. doi:10.1016/j.ctrv.2009.03.004
7. Pantel K, Brakenhoff RH, Brandt B. Detection, clinical relevance and specific biological properties of disseminating tumour cells. Nat Rev Cancer. 2008;8(5):329-340. doi:10.1038/nrc2375
8. Wang FB, Yang XQ, Yang S, Wang BC, Feng MH, Tu JC. A higher number of circulating tumor cells (CTC) in peripheral blood indicates poor prognosis in prostate cancer patients—a meta-analysis. Asian Pac J Cancer Prev. 2011;12(10):2629-2635.
9. Wang L, Balasubramanian P, Chen AP, Kummar S, Evrard YA, Kinders RJ. Promise and limits of the CellSearch platform for evaluating pharmacodynamics in circulating tumor cells. Semin Oncol. 2016;43(4):464-475. doi:10.1053/j.seminoncol.2016.06.004
10. Ramsköld D, Luo S, Wang YC, et al. Full-length mRNA-Seq from single-cell levels of RNA and individual circulating tumor cells. Nat Biotechnol. 2012;30(8):777-782. doi:10.1038/nbt.2282
11. Al-Faqheri W, Thio THG, Qasaimeh MA, Dietzel A, Madou M, Al-Halhouli A. Particle/cell separation on microfluidic platforms based on centrifugation effect: a review. Microfluid Nanofluid. 2017;21(6):102. doi:10.1007/s10404-017-1933-4
12. Nivedita N, Papautsky I. Continuous separation of blood cells in spiral microfluidic devices. Biomicrofluidics. 2013;7(5):54101. doi:10.1063/1.4819275
13. Khodabandeh E, Rozati SA, Joshaghani M, Akbari OA, Akbari S, Toghraie D. Thermal performance improvement in water nanofluid/GNP–SDBS in novel design of double-layer microchannel heat sink with sinusoidal cavities and rectangular ribs. J Therm Anal Calorim. 2019;136(3):1333-1345. doi:10.1007/s10973-018-7826-2
14. Mostafazadeh A, Toghraie D, Mashayekhi R, Akbari OA. Effect of radiation on laminar natural convection of nanofluid in a vertical channel with single- and two-phase approaches. J Therm Anal Calorim. 2019;138(1):779-794. doi:10.1007/s10973-019-08236-2
15. Toghraie D, Mashayekhi R, Arasteh H, Sheykhi S, Niknejadi M, Chamkha AJ. Two-phase investigation of water-Al2O3 nanofluid in a micro concentric annulus under non-uniform heat flux boundary conditions. Int J Numer Methods Heat Fluid Flow. 2019;30(4):1795-1814. doi:10.1108/HFF-11-2018-0628
16. Arasteh H, Mashayekhi R, Goodarzi M, Motaharpour SH, Dahari M, Toghraie D. Heat and fluid flow analysis of metal foam embedded in a double-layered sinusoidal heat sink under local thermal non-equilibrium condition using nanofluid. J Therm Anal Calorim. 2019;138(2):1461-1476. doi:10.1007/s10973-019-08168-x
17. Bazdar H, Toghraie D, Pourfattah F, Akbari OA, Nguyen HM, Asadi A. Numerical investigation of turbulent flow and heat transfer of nanofluid inside a wavy microchannel with different wavelengths. J Therm Anal Calorim. 2020;139(3):2365-2380. doi:10.1007/s10973-019-08637-3
18. Bhagat AAS, Bow H, Hou HW, Tan SJ, Han J, Lim CT. Microfluidics for cell separation. Med Biol Eng Comput. 2010;48(10):999-1014. doi:10.1007/s11517-010-0611-4
19. Pamme N. Continuous flow separations in microfluidic devices. Lab Chip. 2007;7(12):1644-1659. doi:10.1039/B712784G
20. Messaud FA, Sanderson RD, Runyon JR, Otte T, Pasch H, Williams SKR. An overview on field-flow fractionation techniques and their applications in the separation and characterization of polymers. Prog Polym Sci. 2009;34(4):351-368. doi:10.1016/j.progpolymsci.2008.11.001
21. Lu G, Crihfield CL, Gattu S, Veltri LM, Holland LA. Capillary electrophoresis separations of Glycans. Chem Rev. 2018;118(17):7867-7885. doi:10.1021/acs.chemrev.7b00669
22. Kurita M, Matsumoto D, Shigeura T, et al. Influences of centrifugation on cells and tissues in liposuction aspirates: optimized centrifugation for Lipotransfer and cell isolation. Plast Reconstr Surg. 2008;121(3):1033-1041. doi:10.1097/01.prs.0000299384.53131.87
23. Gascoyne PRC, Shim S. Isolation of circulating tumor cells by Dielectrophoresis. Cancer. 2014;6(1):545-579. doi:10.3390/cancers6010545
24. Li Y, Dalton C, John Crabtree H, Nilsson G, Kaler KVIS. Continuous dielectrophoretic cell separation microfluidic device. Lab Chip. 2007;7(2):239-248. doi:10.1039/B613344D
25. Wang X, Chen S, Kong M, et al. Enhanced cell sorting and manipulation with combined optical tweezer and microfluidic chip technologies. Lab Chip. 2011;11(21):3656-3662. doi:10.1039/C1LC20653B
26. Adams JD, Ebbesen CL, Barnkob R, Yang AHJ, Soh HT, Bruus H. High-throughput, temperature-controlled microchannel acoustophoresis device made with rapid prototyping. J Micromech Microeng. 2012;22(7):075017. doi:10.1088/0960-1317/22/7/075017
27. Robert D, Pamme N, Conjeaud H, Gazeau F, Iles A, Wilhelm C. Cell sorting by endocytotic capacity in a microfluidic magnetophoresis device. Lab Chip. 2011;11(11):1902-1910. doi:10.1039/C0LC00656D
28. Yan S, Zhang J, Yuan D, Li W. Hybrid microfluidics combined with active and passive approaches for continuous cell separation. Electrophoresis. 2017;38(2):238-249. doi:10.1002/elps.201600386
29. Yamada M, Nakashima M, Seki M. Pinched flow fractionation: continuous size separation of particles utilizing a laminar flow profile in a pinched microchannel. Anal Chem. 2004;76(18):5465-5471. doi:10.1021/ac049863r
30. Ahasan K, Landry CM, Chen X, Kim JH. Effect of angle-of-attacks on deterministic lateral displacement (DLD) with symmetric airfoil pillars.

Biomed Microdevices. 2020;22(2):42. doi:10.1007/s10544-020-00496-2
31. Song S, Choi S. Design rules for size-based cell sorting and sheathless cell focusing by hydrophoresis. J Chromatogr A. 2013;1302:191-196. doi:10.1016/j.chroma.2013.06.030
32. Carlo DD. Inertial microfluidics. Lab Chip. 2009;9(21):3038-3046. doi:10.1039/B912547G
33. Zhang J, Yan S, Yuan D, et al. Fundamentals and applications of iner-tial microfluidics: a review. Lab Chip. 2015;16(1):10-34. doi:10.1039/C5LC01159K
34. Aghaamoo M, Aghilinejad A, Chen X, Xu J. On the design of deterministic dielectrophoresis for continuous separation of circulating tumor cells from peripheral blood cells. Electrophoresis. 2019;40(10):1486-1493. doi:10.1002/elps.201800459
35. Shim S, Stemke-Hale K, Noshari J, Becker FF, Gascoyne PRC. Dielectrophoresis has broad applicability to marker-free isolation of tumor cells from blood by microfluidic systems. Biomicrofluidics. 2013;7(1):11808. doi:10.1063/1.4774307
36. Yan S, Zhang J, Yuan Y, et al. A hybrid dielectrophoretic and hydrophoretic microchip for particle sorting using integrated prefocusing and sorting steps. Electrophoresis. 2015;36(2):284-291. doi:10.1002/elps.201400397
37. Seo HK, Kim YH, Kim HO, Kim YJ. Hybrid cell sorters for on-chip cell separation by hydrodynamics and magnetophoresis. J Micromech Microeng. 2010;20(9). doi:10.1088/0960-1317/20/9/095019
38. Zhang J, Yuan D, Zhao Q, et al. Tunable particle separation in a hybrid dielectrophoresis (DEP)- inertial microfluidic device. Sens Actuators B. 2018;267:14-25. doi:10.1016/j.snb.2018.04.020
39. Alazzam A, Mathew B, Alhammadi F. Novel microfluidic device for the continuous separation of cancer cells using dielectrophoresis. J Sep Sci. 2017;40(5):1193-1200. doi:10.1002/jssc.201601061
40. Khan M, Chen X. Numerical study of dielectrophoresis-modified inertial migration for overlapping sized cell separation. Electrophoresis. 2022;43(7–8):879-891. doi:10.1002/elps.202100187
41. Islam MS, Uddin MR, Chen X. Circulating tumor cell separation in a Zigzag Channel using Dielectrophoresis based inertial microfluidics. American Society of Mechanical Engineers Digital Collection. Proceedings of the 2022 ASME IMECE Conference. American Society of Mechanical Engineers; 2023. doi:10.1115/IMECE2022-95384
42. Hur SC, Brinckerhoff TZ, Walthers CM, Dunn JCY, Carlo DD. Label-free enrichment of adrenal cortical progenitor cells using inertial microfluidics. PLOS One. 2012;7(10):e46550. doi:10.1371/journal.pone.0046550
43. Bhagat AAS, Kuntaegowdanahalli SS, Kaval N, Seliskar CJ, Papautsky I. Inertial microfluidics for sheath-less high-throughput flow cytometry. Biomed Microdevices. 2010;12(2):187-195. doi:10.1007/s10544-009-9374-9
44. Bhagat AAS, Kuntaegowdanahalli SS, Papautsky I. Continuous particle separation in spiral microchannels using dean flows and differential migration. Lab Chip. 2008;8(11):1906-1914. doi:10.1039/B807107A
45. Guzniczak E, Krüger T, Bridle H, Jimenez M. Limitation of spiral microchannels for particle separation in heterogeneous mixtures: impact of particles' size and deformability. Biomicrofluidics. 2020;14(4):044113. doi:10.1063/5.0009673
46. Ying Y, Lin Y. Inertial focusing and separation of particles in similar curved channels. Sci Rep. 2019;9(1):16575. doi:10.1038/s41598-019-52983-z
47. Jiang D, Ni C, Tang W, Huang D, Xiang N. Inertial microfluidics in contraction–expansion microchannels: a review. Biomicrofluidics. 2021;15(4):041501. doi:10.1063/5.0058732
48. Xiang N, Ni Z. Inertial microfluidics: current status, challenges, and future opportunities. Lab Chip. 2022;22(24):4792-4804. doi:10.1039/D2LC00722C
49. Tang W, Zhu S, Jiang D, Zhu L, Yang J, Xiang N. Channel innovations for inertial microfluidics. Lab Chip. 2020;20(19):3485-3502. doi:10.1039/D0LC00714E
50. Cha H, Fallahi H, Dai Y, et al. Multiphysics microfluidics for cell manipulation and separation: a review. Lab Chip. 2022;22(3):423-444. doi:10.1039/D1LC00869B
51. Afsaneh H, Mohammadi R. Microfluidic platforms for the manipulation of cells and particles. Talanta Open. 2022;5:100092. doi:10.1016/j.talo.2022.100092
52. Xuan X, Zhu J, Church C. Particle focusing in microfluidic devices. Microfluid Nanofluid. 2010;9(1):1-16. doi:10.1007/s10404-010-0602-7
53. Lee MG, Choi S, Park JK. Inertial separation in a contraction–expansion array microchannel. J Chromatogr A. 2011;1218(27):4138-4143. doi:10.1016/j.chroma.2010.11.081
54. Bhagat AAS, Hou HW, Li LD, Lim CT, Han J. Pinched flow coupled shear-modulated inertial microfluidics for high-throughput rare blood cell separation. Lab Chip. 2011;11(11):1870-1878. doi:10.1039/C0LC00633E
55. Shamloo A, Abdorahimzadeh S, Nasiri R. Exploring contraction–expansion inertial microfluidic-based particle separation devices integrated with curved channels. AIChE Journal. 2019;65(11):e16741. doi:10.1002/aic.16741
56. Vona G, Sabile A, Louha M, et al. Isolation by size of epithelial tumor cells: a new method for the Immunomorphological and molecular characterization of circulating tumor cells. Am J Pathol. 2000;156(1):57-63. doi:10.1016/S0002-9440(10)64706-2
57. Hyun KA, Kwon K, Han H, Kim SI, Jung HI. Microfluidic flow fractionation device for label-free isolation of circulating tumor cells (CTCs) from breast cancer patients. Biosens Bioelectron. 2013;40(1):206-212. doi:10.1016/j.bios.2012.07.021
58. Marrinucci D, Bethel K, Luttgen M, Bruce RH, Nieva J, Kuhn P. Circulating tumor cells from well-differentiated lung adenocarcinoma retain cytomorphologic features of primary tumor type. Arch Pathol Lab Med. 2009;133(9):1468-1471. doi:10.5858/133.9.1468
59. Asmolov ES. The inertial lift on a spherical particle in a plane Poiseuille flow at large channel Reynolds number. J Fluid Mech. 1999;381:63-87. doi:10.1017/S0022112098003474
60. Di Carlo D, Edd JF, Humphry KJ, Stone HA, Toner M. Particle segregation and dynamics in confined flows. Phys Rev Lett. 2009;102(9):094503. doi:10.1103/PhysRevLett.102.094503
61. Di Carlo D, Irimia D, Tompkins RG, Toner M. Continuous inertial focusing, ordering, and separation of particles in microchannels. Proc Natl Acad Sci U S A. 2007;104(48):18892-18897. doi:10.1073/pnas.0704958104
62. Dean WR, Chapman S. Fluid motion in a curved channel. Proceedings of the Royal Society of London Series A, Containing Papers of a Mathematical and Physical Character. 1928;121(787):402-420. doi:10.1098/rspa.1928.0205
63. Zhu J, Tzeng TRJ, Xuan X. Continuous dielectrophoretic separation of particles in a spiral microchannel. Electrophoresis. 2010;31(8):1382-1388. doi:10.1002/elps.200900736
64. Jones TB. Electromechanics of Particles. Cambridge University Press; 1995. doi:10.1017/CBO9780511574498
65. Islam MS, Hakim SM, Ali M, Islam MQ. Numerical investigation on boundary layer control through moving surface in NACA 0012 airfoil. AIP Conference Proceedings. 2017;1851(1):20111. doi:10.1063/1.4984740
66. Scala F. Fluidized Bed Technologies for Near-Zero Emission Combustion and Gasification. Woodhead Publishing Limited; 2013. doi:10.1533/9780857098801
67. Waheed W, Sharaf OZ, Alazzam A, Abu-Nada E. Dielectrophoresis-field flow fractionation for separation of particles: a critical review. J Chromatogr A. 2021;1637:461799. doi:10.1016/j.chroma.2020.461799
68. Kim D, Sonker M, Ros A. Dielectrophoresis: from molecular to micrometer-scale Analytes. Anal Chem. 2019;91(1):277-295. doi:10.1021/acs.analchem.8b05454

69. Lee MG, Choi S, Kim HJ, et al. Inertial blood plasma separation in a contraction–expansion array microchannel. Appl Phys Lett. 2011; 98(25):253702. doi:10.1063/1.3601745
70. Han SI, Joo YD, Han KH. An electrorotation technique for measuring the dielectric properties of cells with simultaneous use of negative quadrupolar dielectrophoresis and electrorotation. Analyst. 2013; 138(5):1529-1537. doi:10.1039/C3AN36261B
71. Prinyakupt J, Pluempitiwiriyawej C. Segmentation of white blood cells and comparison of cell morphology by linear and naïve Bayes classifiers. Biomed Eng Online. 2015;14(1):63. doi:10.1186/s12938-015-0037-1
72. Yuan D, Tan SH, Zhao Q, et al. Sheathless Dean-flow-coupled elasto-inertial particle focusing and separation in viscoelastic fluid. RSC Adv. 2017;7(6):3461-3469. doi:10.1039/C6RA25328H
73. Warkiani ME, Tay AKP, Khoo BL, Xiaofeng X, Han J, Lim CT. Malaria detection using inertial microfluidics. Lab Chip. 2015;15(4):1101-1109. doi:10.1039/c4lc01058b
74. Sim TS, Kwon K, Park JC, Lee JG, Jung HI. Multistage-multiorifice flow fractionation (MS-MOFF): continuous size-based separation of microspheres using multiple series of contraction/expansion microchannels. Lab Chip. 2010;11(1):93-99. doi:10.1039/C0LC00109K
75. Wu Z, Chen Y, Wang M, Chung AJ. Continuous inertial microparticle and blood cell separation in straight channels with local microstructures. Lab Chip. 2016;16(3):532-542. doi:10.1039/C5LC01435B
76. Rafeie M, Zhang J, Asadnia M, Li W, Warkiani ME. Multiplexing slanted spiral microchannels for ultra-fast blood plasma separation. Lab Chip. 2016;16(15):2791-2802. doi:10.1039/C6LC00713A
77. Cruz J, Graells T, Walldén M, Hjort K. Inertial focusing with sub-micron resolution for separation of bacteria. Lab Chip. 2019;19(7): 1257-1266. doi:10.1039/C9LC00080A
78. Moon HS, Kwon K, Kim SI, et al. Continuous separation of breast cancer cells from blood samples using multi-orifice flow fractionation (MOFF) and dielectrophoresis (DEP). Lab Chip. 2011;11(6):1118-1125. doi:10.1039/C0LC00345J
79. Lu J, Barrios CA, Dickson AR, Nourse JL, Lee AP, Flanagan LA. Advancing practical usage of microtechnology: a study of the functional consequences of dielectrophoresis on neural stem cells. Integr Biol. 2012;4(10):1223-1236. doi:10.1039/c2ib20171b

How to cite this article: Islam MS, Chen X. Continuous CTC separation through a DEP-based contraction–expansion inertial microfluidic channel. Biotechnol. Prog. 2023;39(4): e3341. doi:10.1002/btpr.3341